# FRICTION MODELS FOR THE ROLLING DISK

**Remco I. Leine**
Center of Mechanics
IMES, ETH Zurich
Switzerland
remco.leine@imes.mavt.ethz.ch

**Cédric Le Saux**
Center of Mechanics
IMES, ETH Zurich
Switzerland

**Christoph Glocker**
Center of Mechanics
IMES, ETH Zurich
Switzerland
christoph.glocker@imes.mavt.ethz.ch

**Abstract**

In this paper we are interested in the dynamics and numerical treatment of a rolling disk on a flat support. The objective of the paper is to develop a numerical model which is able to simulate the dynamics of a rolling disk taking into account frictional resistance against sliding, pivoting and rolling. A mechanical model of a rolling disk is presented in the framework of Non-smooth Dynamics. In an analytical study, approximations are derived for the energy decay of the system during the final stage of the motion for various kinds of frictional dissipation models. Finally, the numerical and analytical results are discussed and compared with experimental results available in literature.

**Key words**

unilateral contact, friction, time-stepping method, Euler disk, set-valued force laws.

## 1 Introduction

The theoretical framework developed during the last decades in the fields of Numerical Analysis and Non-smooth Dynamics provides the basis for the efficient numerical simulation of multi-body systems submitted to multiple unilateral contact constraints with friction. When dealing with multi-body systems submitted to many unilateral contact constraints, the so-called time-stepping approach has proven its efficiency and robustness (Moreau, 1988; Jean, 1999). The time-stepping method permits us to study various kinds of mechanical systems in Civil Engineering (granular materials), dynamics of machines (turbine blade dampers), robotics (walking robots) and mechanisms (electrical circuit-breakers). However, unilateral contact between an object with a flat side of rounded contour and a plane, like that of a bottle on a table, is still a topic of research. Such a type of contact can for instance be found in grinding machines and the transportation of cylindrical objects on a conveyor belt. Systems with such a type of contact undergo a specific type of motion, as is described by a scientific toy called the 'Euler Disk'. The Euler Disk consists of a metal disk, about 75 mm in diameter and a thickness of 12 mm, which can spin on a slightly concave mirror, called the support. More commonly, a similar kind of motion, although with more damping, is that of a coin spinning on a table. This type of motion involves an energy decrease to zero in a finite time accompanied by a certain kind of singularity. In the course of the motion, both the inclination of the disk with respect to the support and its angular velocity decrease to zero, while the relative velocity of the contact point with respect to the disk tends to infinity in the final stage of the motion. The spinning disk on a flat support, which constitutes the simplest example of this specific type of motion regarding the shape of the body, has often been discussed theoretically since the $19^{\text{th}}$ century up to now (Appell, 1900; Moffatt, 2000; McDonald and McDonald, 2001; Easwar *et al.*, 2002; Borisov *et al.*, 2003; Stanislavsky and Weron, 2001; O'Reilly, 1996; Kessler and O'Reilly, 2002).

The objective of the current paper is to develop a numerical model which is able to simulate the dynamics of a rolling disk taking into account the unilateral contact with a flat rigid support, collisions, stick-slip transitions and other frictional effects between disk and support. The mechanical model of a rolling disk is presented in the framework of Non-smooth Dynamics (Moreau, 1988; Glocker, 2001; Leine and Nijmeijer, 2004). Moreover, we want to study the dynamics of a rolling disk by using the numerical model and by an analytical study and to compare those results with experimental results available in literature.

## 2 Mechanical model

We will use the following notation. The displacement of point $B$ relative to point $A$ is expressed by the vector $\boldsymbol{r}_{AB}$. The term $\boldsymbol{v}_B$ denotes the velocity of point $B$, i.e. $\boldsymbol{v}_B = \dot{\boldsymbol{r}}_{AB}$ if $A$ is not moving. Only orthonormal frames are used, which we write as $C = (B, \boldsymbol{e}_x^C, \boldsymbol{e}_y^C, \boldsymbol{e}_z^C)$. The angular velocity of frame $C$ relative to another frame $D$ is denoted by $\boldsymbol{\omega}_{DC}$. The

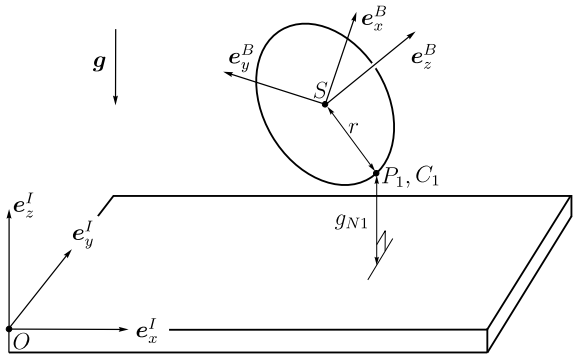


Figure 1. Mechanical system.

angular velocity of a body is thus $\boldsymbol{\omega}_{IB}$, if $B$ denotes a body-fixed frame and $I$ is an inertial frame. The components of a vector $\boldsymbol{a}$ associated with a frame $D$ are denoted ${}_D\boldsymbol{a}$. The velocity ${}_B\boldsymbol{v}_D$ of point $D$ written down in frame $B$ is then obtained by Euler's formula ${}_B\boldsymbol{v}_D = {}_B\dot{\boldsymbol{r}}_{AD} + {}_B\boldsymbol{\omega}_{IB} \times {}_B\boldsymbol{r}_{AD}$, if $A$ is not moving and $I$ denotes the inertial frame. The general version of Euler's formula reads ${}_B(\dot{\boldsymbol{a}}) = {}_B\dot{\boldsymbol{a}} + {}_B\boldsymbol{\omega}_{IB} \times {}_B\boldsymbol{a}$ and is applied in Section 4 on the linear momentum $\bar{\boldsymbol{p}}$ and on the angular momentum $\bar{\boldsymbol{N}}_S$.

The mechanical system under consideration consists of a disk $\Omega$ with radius $r$, mass $m$ and centre of mass $S$, which can be in contact with a table during its motion. The system is modelled as simply as possible, in order to show only the main physical phenomena of interest, and the disk is therefore considered to be infinitely thin. Both the disk and table are considered to be perfectly rigid. An absolute coordinate frame $I = (O, \boldsymbol{e}_x^I, \boldsymbol{e}_y^I, \boldsymbol{e}_z^I)$ is attached to the table and a body fixed coordinate frame $B = (S, \boldsymbol{e}_x^B, \boldsymbol{e}_y^B, \boldsymbol{e}_z^B)$ is attached to the disk such that $\boldsymbol{e}_z^B$ is the axis of revolution (Figure 1). The disk has principal moments of inertia $A = B = \frac{mr^2}{4}$ and $C = \frac{mr^2}{2}$ with respect to $S$ along the axes $(\boldsymbol{e}_x^B, \boldsymbol{e}_y^B, \boldsymbol{e}_z^B)$ respectively. The inertia tensor of the disk with respect to the centre of mass $S$ is denoted by $\boldsymbol{\Theta}_S$. Gravity is denoted by $\boldsymbol{g}$.

### 2.1 System parametrization

The disk is allowed to undergo arbitrary rotations. We parameterize the orientation of the disk with Euler parameters (unit quaternions). For each possible configuration of the body, the absolute orientation of $\Omega$ may be defined by the coordinate transformation $\mathcal{R} : (\boldsymbol{e}_x^I, \boldsymbol{e}_y^I, \boldsymbol{e}_z^I) \mapsto (\boldsymbol{e}_x^B, \boldsymbol{e}_y^B, \boldsymbol{e}_z^B)$, which can be accomplished by a finite rotation of an angle $\chi$ around an axis which is specified by the unit vector $\boldsymbol{n}$. We denote by $n_i$ the three components of ${}_I\boldsymbol{n}$, i.e. the three components of $\boldsymbol{n}$ in the basis $(\boldsymbol{e}_x^I, \boldsymbol{e}_y^I, \boldsymbol{e}_z^I)$. Each rotation $(\boldsymbol{n}, \chi)$ is associated with a unit quaternion, represented in the following by the 4-tuple $\boldsymbol{p}$ which components, $e_0 = \cos\frac{\chi}{2}$ and $e_i = n_i \sin\frac{\chi}{2}$ for $i = 1, 2, 3$, are called the Euler parameters. We will use the abbreviation $\boldsymbol{e} = \left[e_1, e_2, e_3\right]^{\mathrm{T}}$. The Euler parameters fulfill the relationship

$$\boldsymbol{p}^{\mathrm{T}}\boldsymbol{p} = 1, \text{ with } \boldsymbol{p} = \left[e_0 \ \boldsymbol{e}^{\mathrm{T}}\right]^{\mathrm{T}}. \tag{1}$$

The rotation transformation $\mathcal{R}$, which identifies with a linear mapping with associated matrix $\boldsymbol{R} = [R_{ij}] = (2e_0^2 - 1)\boldsymbol{I}_3 + 2(\boldsymbol{e}\boldsymbol{e}^{\mathrm{T}} + e_0\tilde{\boldsymbol{e}})$, relates the global components ${}_I\boldsymbol{s}$ of a vector $\boldsymbol{s}$ to its body-fixed components ${}_B\boldsymbol{s}$ as ${}_I\boldsymbol{s} = \boldsymbol{R}\,{}_B\boldsymbol{s}$. We parameterize the body $\Omega$ using a set of 7 generalized coordinates composed of three translational coordinates ${}_I\boldsymbol{r}_{OS}$, being the absolute coordinates of the centre of mass $S$, and four rotational coordinates $\boldsymbol{p}$, being the Euler parameters. Introducing the generalized coordinate vector

$$\boldsymbol{q} = \begin{bmatrix} {}_I\boldsymbol{r}_{OS} \\ \boldsymbol{p} \end{bmatrix} \in \mathbb{R}^7, \tag{2}$$

a Lagrangian description of the motion can be written in the form ${}_I\boldsymbol{r}_{OM}(\boldsymbol{q}) = {}_I\boldsymbol{r}_{OS} + \boldsymbol{R}\,{}_B\boldsymbol{r}_{SM}$ $\forall\ M \in \Omega$. This equation must be considered together with the constraint (1). Differentiation leads to the Eulerian description of the motion ${}_I\dot{\boldsymbol{r}}_{OM} = {}_I\dot{\boldsymbol{r}}_{OS} + \dot{\boldsymbol{R}}\,{}_B\boldsymbol{r}_{MS}$ $\forall\ M \in \Omega$, with the relations $\dot{\boldsymbol{R}} = {}_I\tilde{\boldsymbol{\omega}}_{IB}\,\boldsymbol{R}$ and $\dot{\boldsymbol{R}} = \boldsymbol{R}\,{}_B\tilde{\boldsymbol{\omega}}_{IB}$, where $\tilde{\boldsymbol{\omega}}_{IB}$ is the skew-symmetric operator associated with the absolute angular velocity of the body $\boldsymbol{\omega}_{IB}$. Subsequently, we introduce the generalized velocity vector $\boldsymbol{u}$, which gathers the absolute coordinates of the global velocity of the centre of mass ${}_I\dot{\boldsymbol{r}}_{OS}$ and the body-fixed coordinates of the absolute angular velocity vector ${}_B\boldsymbol{\omega}_{IB}$,

$$\boldsymbol{u} = \begin{bmatrix} {}_I\dot{\boldsymbol{r}}_{OS} \\ {}_B\boldsymbol{\omega}_{IB} \end{bmatrix} \in \mathbb{R}^6. \tag{3}$$

### 2.2 Contact kinematics

During the time-evolution of the system, the disk can be in contact with the table. The unilateral contact between disk and table is assumed to be of the type point–surface. A single contact constraint is not able to describe the static equilibrium of a disk lying horizontally on the table. We therefore model the disk with three unilateral contact constraints. For an arbitrary configuration of the disk, we define three points on the contour of the disk which are candidates to contact. Subsequently, we derive the normal gap functions $g_{Nj}(\boldsymbol{q})$ associated with the three unilateral contact constraints under consideration $(j = 1, 2, 3)$. It must hold that $g_{Nj}(\boldsymbol{q}) \geq 0$ to avoid penetration.

**2.2.1 Derivation of gap functions** We first consider a non-horizontal configuration of the disk $(R_{33} \neq 1)$. We define the point $C_1$ as the point on the contour of the disk which has a minimal height with respect to the plane of the table. If the disk is above the table, then $C_1$ is the closest point to the table. Let $\boldsymbol{e}_x^K$ be

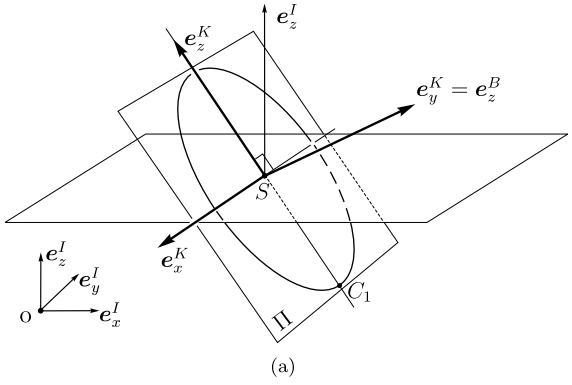


(a)

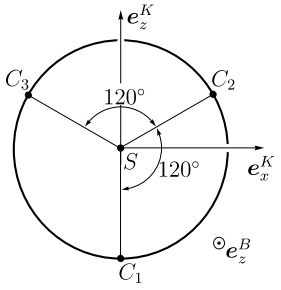


(b)

Figure 2. Contacts point $C_1$, $C_2$ and $C_3$.

a unit directional vector of the intersection line of the plane $\Pi$ of the disk and the horizontal plane $(S, \boldsymbol{e}_x^I, \boldsymbol{e}_y^I)$ (Figure 2), i.e. $\boldsymbol{e}_x^K = -(\boldsymbol{e}_z^I \times \boldsymbol{e}_z^B)/\|\boldsymbol{e}_z^I \times \boldsymbol{e}_z^B\|$ with $\|\boldsymbol{e}_z^I \times \boldsymbol{e}_z^B\| = \sqrt{1 - R_{33}^2}$. The direction in the plane $\Pi$ with the largest inclination with respect to the plane $(S, \boldsymbol{e}_x^I, \boldsymbol{e}_y^I)$ is characterized by the unit vector $\boldsymbol{e}_z^K = -\boldsymbol{e}_z^B \times \boldsymbol{e}_x^K = \left(\boldsymbol{e}_z^I - R_{33}\boldsymbol{e}_z^B\right)/\sqrt{1 - R_{33}^2}$. The point $C_1$ on the contour of the disk which has a minimal height with respect to the plane, is defined by $\boldsymbol{r}_{SC_1} = -r\, \boldsymbol{e}_z^K$. Based on the definition of $C_1$, we introduce two other points $C_2$ and $C_3$ on the contour of the disk, being candidates of contact (Figure 2) defined by $\boldsymbol{r}_{SC_2} = -\frac{1}{2}\, \boldsymbol{r}_{SC_1} + \frac{\sqrt{3}}{2}\left(\boldsymbol{e}_z^B \times \boldsymbol{r}_{SC_1}\right)$, and $\boldsymbol{r}_{SC_3} = -\frac{1}{2}\, \boldsymbol{r}_{SC_1} - \frac{\sqrt{3}}{2}\left(\boldsymbol{e}_z^B \times \boldsymbol{r}_{SC_1}\right)$. The gap functions $g_{Nj}$, associated with the three contact points $C_j$, with $\boldsymbol{r}_{C_j} = \boldsymbol{r}_S + \boldsymbol{r}_{SC_j}$, are defined as $g_{Nj}(\boldsymbol{q}) = \boldsymbol{e}_z^I \cdot \boldsymbol{r}_{C_j}$ $(j = 1, 2, 3)$ and can be expressed in the form $g_{N1}(\boldsymbol{q}) = z_S - r\sqrt{1 - R_{33}^2}$ and $g_{N2}(\boldsymbol{q}) = g_{N3}(\boldsymbol{q}) = z_S + \frac{r}{2}\sqrt{1 - R_{33}^2}$. The functions $g_{Nj}$ are continuous functions in $\boldsymbol{q}$.

If the disk is parallel to the table, then the proximal point can not be uniquely defined because all points on the disk have the same height $z_S$, and the configuration is said to be singular. In this case ($R_{33} = 1,\ g_{N1} = g_{N2} = g_{N3} = z_S$) the functions $\boldsymbol{r}_{SC_j}(\boldsymbol{q})$ $(j = 1, 2, 3)$ are not defined. The points $C_1$, $C_2$ and $C_3$ can therefore, a priori, be chosen arbitrarily on the contour of the disk. When, at a time-instant $t^*$, the disk passes a horizontal singularity position during its motion, we define the points $C_1$, $C_2$ and $C_3$ by the continuity condition $\boldsymbol{r}_{SC_j}^+(t^*) = \boldsymbol{r}_{SC_j}^-(t^*)$ for $j = 1, 2, 3$, where the upper indices $+$ and $-$ denote the right and left limit at $t^*$ with respect to time $t$.

**2.2.2 Derivation of relative velocities at the contact points** Consider the constrained motion of the disk, such that it is in contact with the table at a single point $C_1$ ($g_{N1} = 0$, $g_{N2} = g_{N3} > 0$). The point $C_1$ moves during the time-evolution of the system along the contour of the disk such that it remains the proximal point on the contour with respect to the table. The absolute velocity of point $C_1$ is obtained by differentiation of $\boldsymbol{r}_{OC_1} = \boldsymbol{r}_{OS} + \boldsymbol{r}_{SC_1}$

$$ {}_B\boldsymbol{v}_{C_1} = \underbrace{{}_B\boldsymbol{v}_S + {}_B\boldsymbol{\omega}_{IB} \times {}_B\boldsymbol{r}_{SC_1}}_{{}_B\boldsymbol{v}_{P_1}} + {}_B\dot{\boldsymbol{r}}_{SC_1}\,. \tag{4} $$

The term ${}_B\boldsymbol{v}_{P_1}$ represents the absolute velocity of the body-fixed point $P_1$ which at time-instance $t$ coincides with point $C_1$. The second term ${}_B\dot{\boldsymbol{r}}_{SC_1} = -r\ {}_B\dot{\boldsymbol{e}}_z^K$ corresponds to the velocity of point $C_1$ relative to the disk. For each non-horizontal configuration of the disk ($R_{33} \neq 1$), the coordinate transformation $B = (\boldsymbol{e}_x^B, \boldsymbol{e}_y^B, \boldsymbol{e}_z^B) \mapsto K = (\boldsymbol{e}_x^K, \boldsymbol{e}_y^K, \boldsymbol{e}_z^K)$ is a rotation $\psi$ around axis $\boldsymbol{e}_z^B$. It therefore holds that ${}_B\dot{\boldsymbol{e}}_z^K = {}_B\boldsymbol{\omega}_{BK} \times {}_B\boldsymbol{e}_z^K = \dot{\psi}\ {}_B\boldsymbol{e}_x^K$, from which follows ${}_B\dot{\boldsymbol{r}}_{SC_1} = -r\dot{\psi}\ {}_B\boldsymbol{e}_x^K$. In addition, by differentiation of ${}_B\boldsymbol{r}_{SC_1}$ we obtain ${}_B\dot{\boldsymbol{r}}_{SC_1} = -r\,(\dot{R}_{32}R_{31} - \dot{R}_{31}R_{32})/(1 - R_{33}^2)\ {}_B\boldsymbol{e}_x^K$. By using $\dot{\boldsymbol{R}} = \boldsymbol{R}\ {}_B\tilde{\boldsymbol{\omega}}_{IB}$, we derive the following expression for $\dot{\psi}$

$$ \begin{aligned} \dot{\psi} &= \frac{\dot{R}_{32}R_{31} - \dot{R}_{31}R_{32}}{1 - R_{33}^2} \\ &= \left[\frac{R_{31}R_{33}}{1 - R_{33}^2}\ \frac{R_{32}R_{33}}{1 - R_{33}^2}\ -1\right]\ {}_B\boldsymbol{\omega}_{IB}\,. \end{aligned} \tag{5} $$

We now introduce a number of velocity quantities for the relative kinematics of the interacting bodies. We first define the time-derivative of the gap function $g_{N1}$. Using the notation $\gamma_{N1} = \dot{g}_{N1}$ with $g_{N1} = \boldsymbol{e}_z^I \cdot \boldsymbol{r}_{C_1}$, and considering (4), it holds that

$$ \gamma_{N1} = \boldsymbol{e}_z^I \cdot \boldsymbol{v}_{C_1} = \dot{z}_S - ({}_I\boldsymbol{e}_z^I)^{\mathrm{T}}\ {}_I\tilde{\boldsymbol{r}}_{SC_1}\ \boldsymbol{R}\ {}_B\boldsymbol{\omega}_{IB}\,. \tag{6} $$

That is to say, when $g_{N1} = 0$, $\gamma_{N1}$ represents the relative velocity of the interacting bodies in the direction $\boldsymbol{e}_z^I$ normal to the contact plane $(\boldsymbol{e}_x^I, \boldsymbol{e}_y^I)$. Secondly, we define the tangential relative velocity $\boldsymbol{\gamma}_{T1}$ of the interacting bodies at contact point $C_1$, as a 2-vector which elements are the first two components of ${}_I\boldsymbol{v}_{P_1}$

$$ \boldsymbol{\gamma}_{T1} = \begin{bmatrix} \dot{x}_S - ({}_I\boldsymbol{e}_x^I)^{\mathrm{T}}\ {}_I\tilde{\boldsymbol{r}}_{SC_1}\ \boldsymbol{R}\ {}_B\boldsymbol{\omega}_{IB} \\ \dot{y}_S - ({}_I\boldsymbol{e}_y^I)^{\mathrm{T}}\ {}_I\tilde{\boldsymbol{r}}_{SC_1}\ \boldsymbol{R}\ {}_B\boldsymbol{\omega}_{IB} \end{bmatrix}. \tag{7} $$

The relative spin vector of the interacting bodies, $\boldsymbol{\omega}_{\mathrm{spin}}$, is a vector normal to the contact plane $\boldsymbol{\omega}_{\mathrm{spin}} = \omega_{\mathrm{spin}}\boldsymbol{e}_z^I$,

with $\omega_{\text{spin}} = \boldsymbol{\omega}_{IB} \cdot \boldsymbol{e}_z^I$. Furthermore, we introduce the spin velocity $\gamma_{\tau 1}$ as the product of the relative spin $\omega_{\text{spin}}$ and some quantity $\epsilon_1$

$$\gamma_{\tau 1} = \epsilon_1 \, \omega_{\text{spin}} = \epsilon_1 ({}_I\boldsymbol{e}_z^I)^{\mathrm{T}} \; {}_I\boldsymbol{\omega}_{IB}, \tag{8}$$

where $\epsilon_1$ is an assumed radius of a hypothetical circular contact area in the $(\boldsymbol{e}_x^I, \boldsymbol{e}_y^I)$-plane. Lastly, we define the relative 'rolling' velocity $\gamma_R$ as the product of minus the radius of the disk and $\dot{\psi}$ (5)

$$\gamma_{R1} = -r \, \dot{\psi} = r \begin{bmatrix} \dfrac{-R_{31}R_{33}}{1-R_{33}^2} & \dfrac{-R_{32}R_{33}}{1-R_{33}^2} & 1 \end{bmatrix} {}_B\boldsymbol{\omega}_{IB} \, .$$

Subsequently, we treat the situation for which the disk, while being in contact, passes a horizontal singularity position at instant $t^\star$ and thereafter moves in the plane of the table ($g_{N1} = g_{N2} = g_{N3} = 0$, and thus $R_{33} = 1$). At such a time-instant $t^\star$, the previous relations for ${}_B\boldsymbol{r}_{SC_j}$ do not hold, and the points $C_1$, $C_2$, $C_3$ are defined by the continuity condition $\boldsymbol{r}_{SC_j}^+(t^\star) = \boldsymbol{r}_{SC_j}^-(t^\star)$, $j = 1,2,3$, in which $\boldsymbol{r}_{SC_j}^-(t^\star)$ is considered to be known. During the subsequent time-evolution (in the plane of the table), the three points $C_1$, $C_2$, $C_3$ are considered to be fixed to the disk. Consequently, the relative velocities $\boldsymbol{\gamma}_{Rj}$, $j = 1,2,3$ are considered to be zero. According to the definition $g_{Nj} = \boldsymbol{e}_z^I \cdot \boldsymbol{r}_{C_j}$, the time-derivative of the gap functions $\gamma_{Nj} = \dot{g}_{Nj}$ $(j = 1,2,3)$ are defined by expressions of the form (6). Similarly, $\gamma_{Tj}$ and $\gamma_{\tau j}$ $(j = 1,2,3)$ are defined by expressions of the form (7) and (8), respectively.

Summarizing, for arbitrary configurations of the disk, we can write the relative velocities $\gamma_{Nj}$, $\boldsymbol{\gamma}_{Tj}$, $\gamma_{\tau j}$ and $\gamma_{Rj}$, for $j = 1,2,3$, as affine functions of $\boldsymbol{u}$, i.e. $\gamma_{Nj} = \boldsymbol{W}_{Nj}^{\mathrm{T}} \boldsymbol{u}$, $\boldsymbol{\gamma}_{Tj} = \boldsymbol{W}_{Tj}^{\mathrm{T}} \boldsymbol{u}$, $\gamma_{\tau j} = \boldsymbol{W}_{\tau j}^{\mathrm{T}} \boldsymbol{u}$ and $\gamma_{Rj} = \boldsymbol{W}_{Rj}^{\mathrm{T}} \boldsymbol{u}$. It can be demonstrated that $\boldsymbol{W}_{N1}$, $\boldsymbol{W}_{N2}$, $\boldsymbol{W}_{N3}$ are three linearly independent vectors, which is of importance especially when dealing with non-interpenetration constraint violations.

### 2.3 Constitutive laws

Associated with each of the relative velocities $\boldsymbol{\gamma}$ are forces $\boldsymbol{\lambda}$ as their dual entities, for which we now introduce certain constitutive laws. These constitutive laws regard unilateral contact, Coulomb-Contensou friction as well as rolling friction, and are formulated as set-valued interaction laws in the framework of convex analysis by applying the concept of normal cone. The index $j$, used to label the contact constraints, is omitted for brevity in the following.

**2.3.1 Contact in normal direction** We assume Signorini's law to hold in the normal direction associated with a unilateral constraint $g_N \geq 0$, $\lambda_N \geq 0$, $g_N \cdot \lambda_N = 0$, where $\lambda_N$ represents the normal contact force. Within the context of non-smooth dynamics we have to allow for temporal discontinuities, e.g. velocity jumps usually associated with collisions. The generalized velocity vector $\boldsymbol{u}$ is assumed to be a function of locally bounded variation on the time-interval $T$ of interest (Moreau, 1988). Such a function possesses a left limit $\boldsymbol{u}^-(t)$ and a right limit $\boldsymbol{u}^+(t)$ at every time-instance $t \in T$. Similarly, a left and right limit exists for the relative velocity $\gamma_N$ considering $\boldsymbol{W}_N$ to be a continuous function of time. For a time-instance $t$ for which $g_N = 0$ and $\lambda_N$ admits a right limit it follows that $\gamma_N^+ \geq 0$, $\lambda_N^+ \geq 0$, $\gamma_N^+ \cdot \lambda_N^+ = 0$, which is Signorini's condition on velocity level. It is possible to prove that if Signorini's condition on velocity level is satisfied for almost every time-instance $t \in T$, and if $g_N \geq 0$ at the initial time-instance $t_0$ then the non-interpenetration of the interacting bodies are satisfied for all $t \in T$ succeeding $t_0$ (see also Proposition 7.1.1. in (Glocker, 2001)). Using concepts of Convex Analysis, we can write Signorini's condition on velocity level in the form

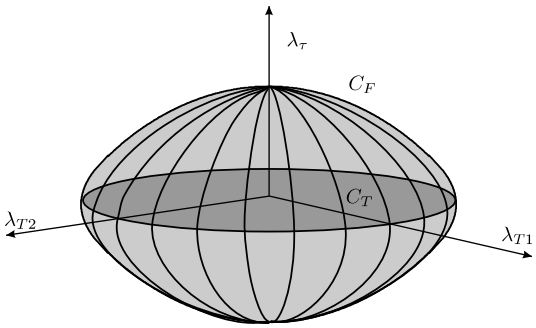


Figure 3. Friction ball $C_F$.

$$-\gamma_N^+ \in N_{C_N}(\lambda_N^+), \tag{9}$$

where $N_{C_N}(\lambda_N^+)$ is the normal cone to $C_N$ at $\lambda_N^+$, with $C_N := \mathbb{R}^+$.

**2.3.2 Coulomb-Contensou friction** Drilling friction is taken into account by using the Coulomb-Contensou friction model (Leine and Glocker, 2003). The Coulomb-Contensou friction model describes the coupled behaviour of spatial sliding friction and drilling friction. The tangential friction force $\boldsymbol{\lambda}_T$ and the normal drilling torque $\tau_N$ are derived from a non-smooth scalar convex (pseudo) potential (dissipation function) expressed in terms of the sliding velocity $\boldsymbol{\gamma}_T$ and spin $\omega_{\text{spin}}$. We assume that the disk locally deforms in the vicinity of a contact such that it has a circular contact surface with radius $\epsilon$ in the contact plane. Moreover, we consider a parabolic normal pressure distribution over the contact area. The Coulomb-Contensou friction model reads for a persistent contact as

$$-\boldsymbol{\gamma}_F \in N_{C_F}(\boldsymbol{\lambda}_F), \tag{10}$$

in which $\boldsymbol{\lambda}_F = \begin{bmatrix}\boldsymbol{\lambda}_T \ \lambda_\tau\end{bmatrix}^{\mathrm{T}}$, $\lambda_\tau = \frac{\tau_N}{\epsilon}$, $\boldsymbol{\gamma}_F = \begin{bmatrix}\boldsymbol{\gamma}_T \ \gamma_\tau\end{bmatrix}^{\mathrm{T}} = \boldsymbol{W}_F^{\mathrm{T}}\,\boldsymbol{u}$ with $\boldsymbol{W}_F = \begin{bmatrix}\boldsymbol{W}_T \ \boldsymbol{W}_\tau\end{bmatrix}$. The convex set $C_F$, shown in Figure 3, is defined in (Leine and Glocker, 2003). The coefficient of friction in the Coulomb-Contensou friction model is denoted by $\mu_F$ and is in general a function of $\boldsymbol{\gamma}_F$. It is important to realize that the frictional sliding force $\boldsymbol{\lambda}_T$ and the normalized drilling torque $\lambda_\tau$ are *coupled* by the Coulomb-Contensou friction law (10). If both the sliding velocity $\boldsymbol{\gamma}_T$ and spin $\omega_{\mathrm{spin}}$ are identically zero, then this case is referred to as 'stick'. If either the sliding velocity $\boldsymbol{\gamma}_T$ or the spin $\omega_{\mathrm{spin}}$ are nonzero, then the contact is in 'slip'.

In the case of a persistent contact, the ratio $\|\boldsymbol{\gamma}_T\|/\mu_F\lambda_N$ is a strictly increasing smooth function of $\|\boldsymbol{\gamma}_T\|/\gamma_\tau$ for non-zero values of $\gamma_\tau = \epsilon\omega_{\mathrm{spin}} \neq 0$. Similarly, the ratio $\lambda_\tau/\mu_F\lambda_N$ is a strictly increasing smooth function of the ratio $\gamma_\tau/\|\boldsymbol{\gamma}_T\|$ for non-zero values of $\boldsymbol{\gamma}_T \neq 0$. For example, this means that $\|\boldsymbol{\gamma}_T\|$ decreases when $\gamma_\tau$ increases for fixed values of $\boldsymbol{\gamma}_T$ and $\mu_F\lambda_N$. This physical effect can be demonstrated by an electric polishing machine used to clean floors. The machine is hard to move when the brushes are not rotating but can easily be pushed over the floor with rotating brushes.

**2.3.3 Contour friction** Classically, the resistance against rolling of two interacting bodies is modelled by the Coulomb's law of rolling friction. This set-valued force law relates a frictional couple transmitted by the contact to the relative velocity of rotation of the two interacting bodies. However, the classical rolling friction law is ambiguous and can lead to contradictions. Here, we will employ another type of rolling friction law, which models resistance against the movement of the contact point along the contour of the disk. We refer to this rolling friction law as the *contour friction model* throughout this paper. The contour friction model for a persistent contact relates the relative (rolling) velocity $\gamma_R$ to a force $\lambda_R$ opposing the movement of the contact point along the contour of the disk

$$-\gamma_R \in N_{C_R}(\lambda_R), \tag{11}$$

in which $C_R := \{v \in \mathbb{R} \mid |v| \leq \mu_R\lambda_N\}$.

## 3 Numerical results

The time-stepping method (Moreau, 1988; Leine and Nijmeijer, 2004; Leine *et al.*, 2005) has been used to simulate the time-evolution of a rolling disk. The following dataset has been used for the simulation. Inertial properties: $m = 0.3048$ kg, $A = B = 1.0716 \times 10^{-4}$ kg m$^2$, $C = 2.1433 \times 10^{-4}$ kg m$^2$, $g = 9.81$ m/s$^2$. Geometrical properties: $r = 3.75 \times 10^{-2}$ m. Contact properties: $\mu_{Fj} = 0.3$, $\epsilon_j = 2 \times 10^{-3}$ m, $\mu_{Rj} = 0.3 \times 10^{-3}$ for $j = 1, 2, 3$. Initially, the disk is considered to be orthogonal to the table and rolling without sliding but with an additional small angular velocity around the $\boldsymbol{e}_x^K$ axis which causes the disk to turn. The stepsize of the numerical scheme is given the fixed value $\Delta t = 10^{-4}$ s.

The results of the simulation with Coulomb-Contensou and contour friction are presented in Figure 4. Immediately after $t = 0$ s, the disk starts to slide laterally (also to pivot) which leads to a decrease in the inclination of the disk and therefore in the potential energy of the system (graphs $(t, g_N)$ and $(t, \beta)$). At time-instant $t = 0.4$ s, when the nutation reaches the value $\beta = 0.45$ rad, the sliding velocity of contact 1 highly increases and subsequently decreases on a short time-interval, as is illustrated by the peak in the graph $(t, \|\boldsymbol{\gamma}_{T1}\|)$. The contour friction force $\lambda_{R1}$ is very small because the contour friction coefficient $\mu_{R1}$ is taken to be a small constant $3 \cdot 10^{-4}$. Meanwhile, the contour rolling velocity $\gamma_{R1}$ is rather small during this part of motion. The dissipation due to contour friction is therefore small with respect to the dissipation due to Coulomb-Contensou friction. The dissipated energy is mostly due to the work done by the tangential contact force. During the subsequent part of the motion, in presence of sliding and spinning, the inclination of the disk with respect to the table and its angular velocity fall down, whereas the velocity of the contact point with respect to the disk $C_1$ is strongly increasing (graphs $(t, \beta)$ and $(t, \dot{\psi})$). When the disk approaches a horizontal configuration, the contour rolling velocity $\gamma_{R1}$ tends to infinity and contour friction becomes the main mechanism of energy dissipation. At time t=13.6 s, as contact 2 and 3 become active, the disk reaches a horizontal equilibrium configuration. Contour friction plays a crucial role in the end phase of the motion and causes the disk to reach a horizontal equilibrium configuration in a finite time.

## 4 Analytical analysis of rolling motion

The simulation of the previous section reveals various dynamic effects. The consideration of an analytical model of the pure rolling motion of the disk permits to give an interpretation of these dynamic effects and therefore contributes to a better understanding of the dynamics of a rolling disk.

The analytical model, presented here, describes the mechanical system under consideration as a disk submitted to a bilateral contact constraint and a sticking condition at contact point $C_1$. We define a parametrization of the disk $(x,\ y,\ \alpha,\ \beta,\ \gamma)$ as illustrated in Figure 6, which accounts for the bilateral contact constraint in normal direction. The sticking condition at contact point $C_1$ can be expressed by means of the two nonholonomic scalar constraints $\dot{x} - y\dot{\alpha} - r\dot{\gamma} = 0$ and $\dot{y} + x\dot{\alpha} = 0$. These conditions permit us to express $\dot{x}$ and $\dot{y}$ as functions of $\dot{\alpha}$, $\dot{\beta}$ and $\dot{\gamma}$. Subsequently, we write the equations of motion using the coordinates $(x,\ y,\ \alpha,\ \beta,\ \gamma)$ and minimal velocities $(\dot{\alpha},\ \dot{\beta},\ \dot{\gamma})$.

First, we derive the angular velocity ${}_K\boldsymbol{\omega}_{IB}$ and the velocity of the center of mass ${}_K\boldsymbol{v}_S$ of the disk, by using

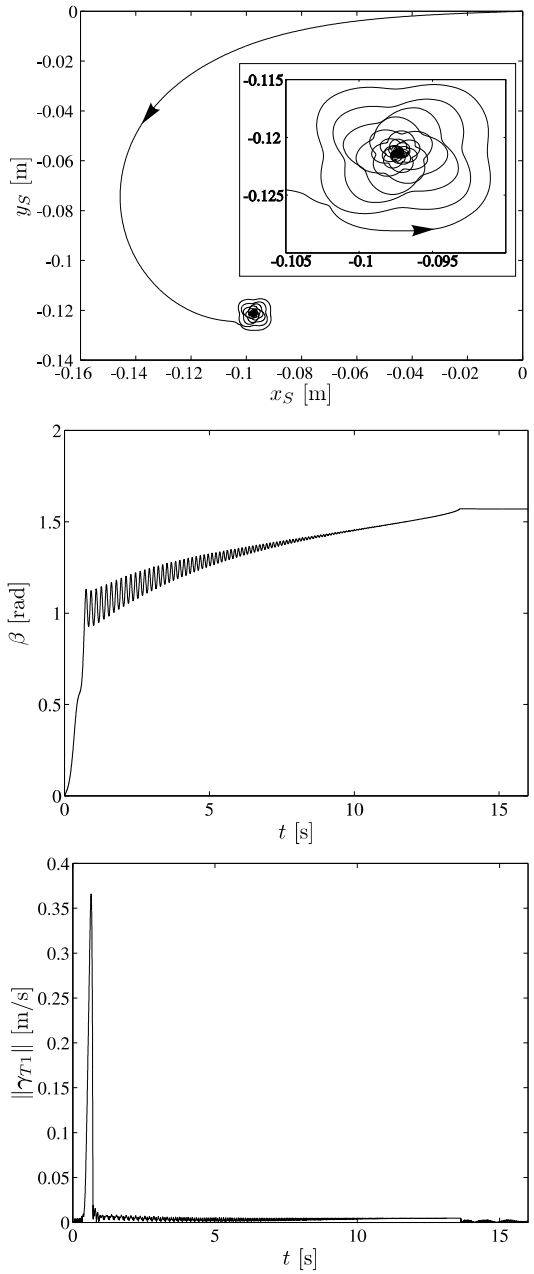


Figure 4. Simulation with Coulomb-Contensou and contour friction.

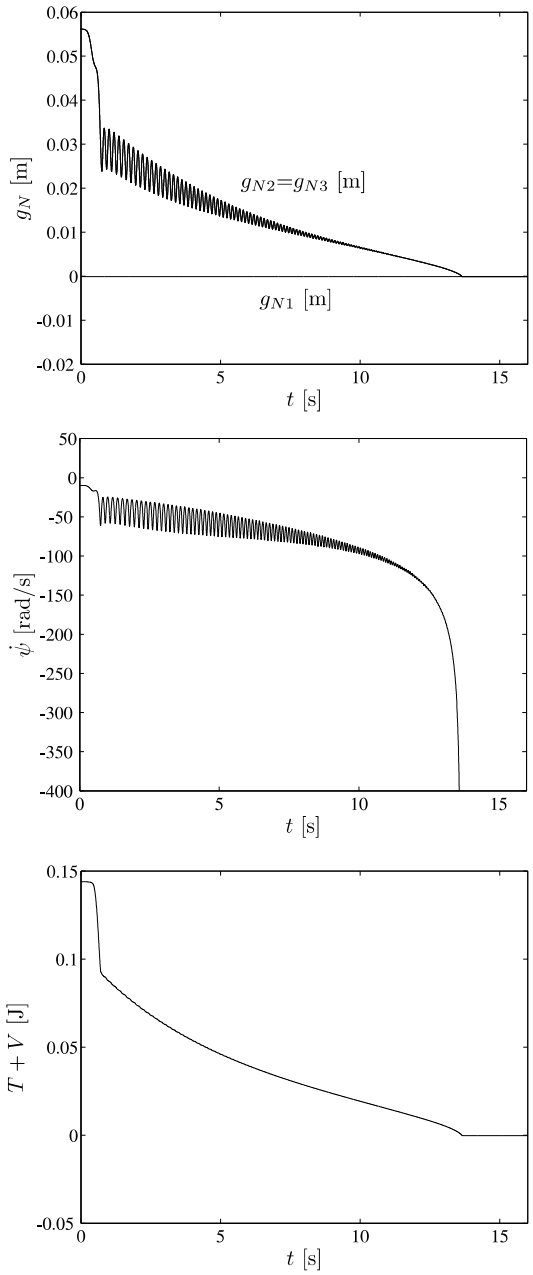


Figure 5. Simulation with Coulomb-Contensou and contour friction.

frame $K = (\boldsymbol{e}_x^K, \boldsymbol{e}_y^K, \boldsymbol{e}_z^K)$,

$$
\begin{aligned}
{}_K\boldsymbol{\omega}_{IB} &= \dot{\alpha}\ {}_K\boldsymbol{e}_z^R + \dot{\beta}\ {}_K\boldsymbol{e}_x^K + \dot{\gamma}\ {}_K\boldsymbol{e}_y^K \\
&= \underbrace{\begin{bmatrix} 0 & 1 & 0 \\ \sin\beta & 0 & 1 \\ \cos\beta & 0 & 0 \end{bmatrix}}_{{}_K\bar{\boldsymbol{J}}_R} \begin{bmatrix} \dot{\alpha} \\ \dot{\beta} \\ \dot{\gamma} \end{bmatrix} \qquad , \\
{}_K\boldsymbol{v}_S = {}_K\boldsymbol{\omega}_{IB} \times {}_K\boldsymbol{r}_{C_1S} &= \underbrace{\begin{bmatrix} r\sin\beta & 0 & r \\ 0 & -r & 0 \\ 0 & 0 & 0 \end{bmatrix}}_{{}_K\bar{\boldsymbol{J}}_S} \begin{bmatrix} \dot{\alpha} \\ \dot{\beta} \\ \dot{\gamma} \end{bmatrix} .
\end{aligned} \tag{12}
$$

Note that frame $K$ is not body-fixed, but moves along with the disk such that the $\boldsymbol{e}_x^K$-axis remains parallel to the table.

Furthermore, we introduce the linear momentum ${}_K\bar{\boldsymbol{p}} = m\,{}_K\boldsymbol{v}_S$ and angular momentum ${}_K\bar{\boldsymbol{N}}_S = {}_K\boldsymbol{\Theta}_S\ {}_K\boldsymbol{\omega}_{IB}$ of the disk. Considering the parameters for the disk $A = B = \frac{mr^2}{4}$ and $C = \frac{mr^2}{2}$, it holds that

$${}_K(\dot{\bar{\boldsymbol{p}}}) = mr \begin{bmatrix} \ddot{\alpha}\sin\beta + \ddot{\gamma} + 2\dot{\alpha}\dot{\beta}\cos\beta \\ -\ddot{\beta} + \dot{\alpha}^2\sin\beta\cos\beta + \dot{\alpha}\dot{\gamma}\cos\beta \\ -\dot{\beta}^2 - \dot{\alpha}^2\sin^2\beta - \dot{\alpha}\dot{\gamma}\sin\beta \end{bmatrix},$$

$${}_K(\dot{\bar{\boldsymbol{N}}}_S) = \tfrac{1}{4}mr^2 \begin{bmatrix} \ddot{\beta} - \dot{\alpha}^2\sin\beta\cos\beta - 2\dot{\alpha}\dot{\gamma}\cos\beta \\ 2\ddot{\alpha}\sin\beta + 2\ddot{\gamma} + 2\dot{\alpha}\dot{\gamma} \\ \ddot{\alpha}\cos\beta + 2\dot{\beta}\dot{\gamma} \end{bmatrix}.$$

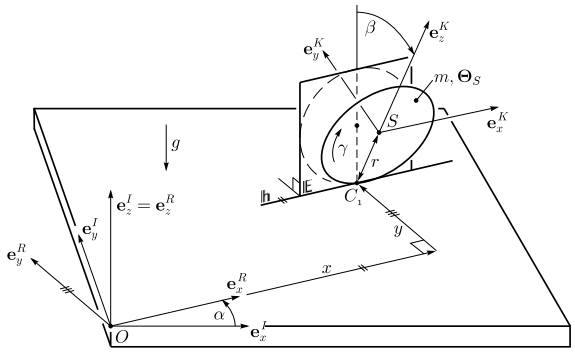


Figure 6. Parametrization of the disk.

Subsequently, we apply the principle of virtual power for virtual velocities which are compatible with the sticking condition. As the constraints are considered to be ideal, only the action of gravity arises in the virtual power of external effort. The action of the gravity on the disk is described by a force ${}_K\boldsymbol{F} = m\tilde{g}r\left[0 - \sin\beta - \cos\beta\right]^{\mathrm{T}}$ and a momentum ${}_K\boldsymbol{M}_S = \mathbf{0}$ with $\tilde{g} = \frac{g}{r}$. From the principle of virtual power follow the projected Newton-Euler equations (Glocker, 2001)

$${}_K\bar{\boldsymbol{J}}_S^{\mathrm{T}}\ \left[{}_K(\dot{\bar{\boldsymbol{p}}}) - {}_K\boldsymbol{F}\right] + {}_K\bar{\boldsymbol{J}}_R^{\mathrm{T}}\ \left[{}_K(\dot{\bar{\boldsymbol{N}}}_S) - {}_K\boldsymbol{M}_S\right] = \mathbf{0},$$

which yield the equations of motion of the disk:

$$\begin{aligned}(5\sin^2\beta + 1)\ddot{\alpha} + 6\ddot{\gamma}\sin\beta + 10\dot{\alpha}\dot{\beta}\sin\beta\cos\beta \\ + 2\dot{\beta}\dot{\gamma}\cos\beta = 0,\end{aligned} \tag{13}$$

$$5\ddot{\beta} - 5\dot{\alpha}^2\sin\beta\cos\beta - 6\dot{\alpha}\dot{\gamma}\cos\beta - 4\tilde{g}\sin\beta = 0, \tag{14}$$

$$6\ddot{\alpha}\sin\beta + 6\ddot{\gamma} + 10\dot{\alpha}\dot{\beta}\cos\beta = 0. \tag{15}$$

### 4.1 Circular rolling motion

We now proceed to analyze a particular type of rolling motion. We consider the type of motion $(x_0(t),\, y_0(t),\, \alpha_0(t),\, \beta_0(t),\, \gamma_0(t))$ for which $x_0 = 0$ and $\beta_0 = \text{const.}$ $(0 < \beta_0 < \frac{\pi}{2})$ in time. It follows that $\dot{x}_0 = \ddot{x}_0 = 0$ and $\dot{\beta}_0 = \ddot{\beta}_0 = 0$. Consequently the sticking conditions $\dot{x} - y\dot{\alpha} - r\dot{\gamma} = 0$ and $\dot{y} + x\dot{\alpha} = 0$ yield $\dot{y}_0 = -x_0\dot{\alpha}_0 = 0 \Rightarrow \dot{y}_0 = \ddot{y}_0 = 0$ ; $y_0 = R$ and $\dot{x}_0 = y_0\dot{\alpha}_0 + r\dot{\gamma}_0 \Rightarrow 0 = R\dot{\alpha}_0 + r\dot{\gamma}_0$. During such a motion, the inclination of the disk $\beta_0$ with respect to the vertical $\boldsymbol{e}_z^I$ and the height of the center of mass, are constant in time. As contact point $C_1$ moves on the contour of the disk (relative motion), it describes on the table (absolute motion) a circular trajectory $(O, R)$ of radius $R$ around the origin $O$ of the inertial frame. The equation $0 = R\dot{\alpha}_0 + r\dot{\gamma}_0$ is the condition for pure rolling, which means that, for a given time-interval of the motion, the arc lengths covered by the contact point $C_1$ on both the perimeter of the circle $(O, R)$ and the perimeter of the disk, are equal. In the following we refer to such motion as *circular rolling motion*. Subtraction of (15)$\cdot \sin\beta_0$ from (13) yields, together with $\dot{\beta}_0 = 0$, to $\ddot{\alpha}_0 = 0$. Consequently, it can be deduced from the pure rolling condition that both $\dot{\alpha}_0$ and $\dot{\gamma}_0$ are constant in time for circular rolling motion. In the following we define $\rho$ as $\rho = \frac{r}{R}$. It follows from the equation of motion (14), and the pure rolling condition written as $\dot{\alpha}_0 = -\rho\dot{\gamma}_0$ that

$$\dot{\gamma}_0^2 = \frac{4\tilde{g}\sin\beta_0}{(6 - 5\rho\sin\beta_0)\rho\cos\beta_0}, \tag{16}$$

with $0 < \rho < \frac{6}{5\sin\beta_0}$.

Subsequently, we study a particular type of circular rolling motion for which, as the disk is rolling on the table, the center of mass $S$ remains on the axis $(O, \boldsymbol{e}_z^I)$. Such type of motion is characterized by $r\sin\beta_0 = R$ or $\rho\sin\beta_0 = 1$, which fulfills the restriction in (16). In this case $\dot{\gamma}^2$ and $\dot{\alpha}^2$ can be written as

$$\dot{\gamma}_0^2 = \frac{4\tilde{g}}{\rho\sqrt{\rho^2 - 1}} \quad \text{and} \quad \dot{\alpha}_0^2 = \rho^2\dot{\gamma}_0^2 = \frac{4\tilde{g}\rho}{\sqrt{\rho^2 - 1}}. \tag{17}$$

Considering (12) together with $\dot{\alpha}_0 = -\rho\dot{\gamma}_0$, $\rho\sin\beta_0 = 1$ and (17) we deduce

$$\| \boldsymbol{\omega}_{IB} \|^2 = 4\tilde{g}\sqrt{1 - \frac{1}{\rho^2}} \quad \text{and} \quad \boldsymbol{v}_S = \mathbf{0},$$

which reveals that the center of mass $S$ is immobile with respect to the inertial frame. We call this type of motion *stationary rolling motion*. In the limit of $\beta_0 \to \frac{\pi}{2}$ it holds that $\rho \to 1$. Consequently, it follows that $\dot{\alpha}_0^2$ and $\dot{\gamma}_0^2 \to +\infty$ while $\boldsymbol{\omega}_{IB} \to \mathbf{0}$. The contact point $C_1$ therefore moves infinitely fast on the circle $(O, R)$ with radius $R \to r$, and moves infinitely fast on the contour of the disk, while the disk does practically not rotate.

### 4.2 Energy decay during the final stage of motion

In the beginning of this analytical analysis we studied the circular rolling motion (without dissipation) of a disk. As a special case, we focused on the stationary rolling motion, for which the center of mass $S$ remains immobile with respect to the inertial frame.

Section 3 shows the numerical simulation of a rolling disk with Coulomb-Contensou and contour friction. The numerical results, in terms of $\boldsymbol{q}(t)$ (2) and $\boldsymbol{u}(t)$ (3), can be expressed in the parametrization $(x, y, \alpha, \beta, \gamma)$ of the analytical model (Figure 6). A number of observations can be made concerning the simulation. During the first phase of the motion, the disk rolls over the table much like the circular rolling motion. However, the system is not conservative due the presence of friction and the movement slowly changes. A short phase of rapid sliding occurs. We observe that the subsequent time-evolution of the disk is much like stationary

rolling motion. As $\beta$ tends to $\pi/2$, the center of mass hardly moves and the relative sliding velocity is becoming small. Moreover, the component $\omega_x = \dot{\beta}$ of the angular velocity along the axis $\boldsymbol{e}_x^R$ (Figure 6) becomes small when compared to the component $\omega_y = \dot{\gamma}\cos\beta$ along the axis $\boldsymbol{e}_y^R$.

In the following, we will study analytically the energy decay of a rolling disk for various kinds of dissipation using the following standing assumptions for the type of motion

A.1 The center of mass is assumed to be almost immobile, i.e. $\rho \sin\beta = 1$.
A.2 We assume $|\ddot{\beta}| \ll \tilde{g}$ and $|\dot{\beta}| \ll |\dot{\alpha}|\cos\beta$.
A.3 The sliding velocity is assumed to be small, i.e. $\dot{\alpha} = -\rho\dot{\gamma}$.
A.4 We assume $\beta$ to be close to $\pi/2$.

The analytically obtained energy decays for different kinds of dissipation will be compared with the energy decay during the final stage of the motion of the corresponding numerical simulations. With assumptions A.1–A.4, it follows from equation of motion (14) that (17) still holds approximately, i.e. $\dot{\gamma}(t) = \dot{\gamma}(\rho(t))$ and $\dot{\alpha}(t) = \dot{\alpha}(\rho(t))$ with $\rho(t) = 1/\sin\beta(t)$. Subsequently, we derive the total energy of the system $E = T + V$ with $V = mgr\cos\beta$ and

$$\begin{aligned} T &= \frac{1}{2} m\, {}_K\boldsymbol{v}_S{}^{\mathrm{T}}\, {}_K\boldsymbol{v}_S + \frac{1}{2}\, {}_K\boldsymbol{\omega}_{IB}{}^{\mathrm{T}}\, {}_K\boldsymbol{\Theta}_S\, {}_K\boldsymbol{\omega}_{IB} \\ &= \frac{1}{2} mr^2 \left( (\dot{\alpha}\sin\beta + \dot{\gamma})^2 + \dot{\beta}^2 \right) \\ &\quad + \frac{1}{2}\left( A\dot{\beta}^2 + C(\dot{\alpha}\sin\beta + \dot{\gamma})^2 + A\dot{\alpha}^2\cos^2\beta \right). \end{aligned}$$

Using the above assumptions, we approximate the total energy by the expression $E = \frac{1}{2}A\dot{\alpha}^2\cos^2\beta + mgr\cos\beta$, in which only the major terms have been taken into account. An expression for the energy as a function of $\beta$

$$E = \frac{3}{2} mr^2 \tilde{g}\cos\beta \tag{18}$$

follows from the substitution of (17) and $A = \frac{1}{4}mr^2$. In the following, we express, for different kinds of friction models, the power as a function of energy, i.e. $\dot{E} = f(E)$. The corresponding power–energy relations define a time-evolution of the system, which can be shown to verify the standing assumptions A.1-A.4.

**4.2.1 Contour friction model** First we consider a model of rolling friction called contour friction (Section 2.3.3), which relates the velocity of the contact point on the contour of the disk $\gamma_R$ to a friction force by relation (11). Considering the parametrization of the disk $(x, y, \alpha, \beta, \gamma)$ it holds that $\gamma_R = -r\dot{\gamma}$. If we choose a dry contour friction law, as used in Section 2.3.3, then the dissipation rate reads as $\dot{E} = -\mu_R\lambda_N|\gamma_R| = -r\mu_R\lambda_N|\dot{\gamma}|$. The assumptions A.2 and A.4 allow us to approximate the normal contact force with $\lambda_N = mg$. We now have to express $\dot{\gamma}$ as a function of $E$. Using (17), (18) and $\rho = 1/\sqrt{1-\cos^2\beta}$, it holds that

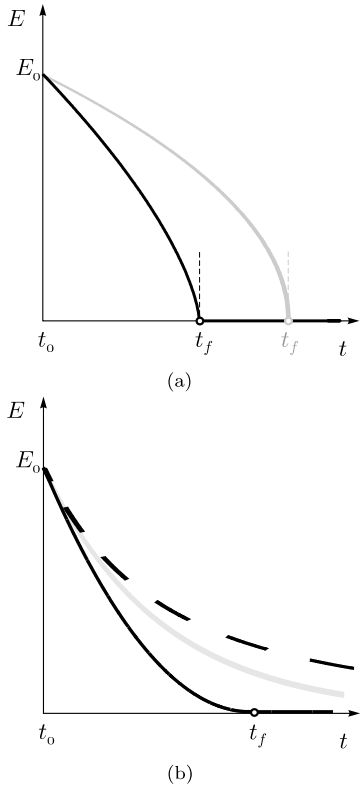


Figure 7. Energy decay for (a) contour friction (dry = black, viscous = grey), (b) classical rolling friction (dry = black, viscous = grey) and Contensou friction (dashed).

$$\begin{aligned} \dot{\gamma}^2 &= \frac{4\tilde{g}}{\rho\sqrt{\rho^2-1}} = \frac{4\tilde{g}(1-\cos^2\beta)}{\cos\beta} \\ &= \frac{4\tilde{g}\left(1 - \left(\frac{2E}{3mr^2\tilde{g}}\right)^2\right)}{\left(\frac{2E}{3mr^2\tilde{g}}\right)}. \end{aligned} \tag{19}$$

It follows from assumption A.4 that $E \ll \frac{3}{2}mr^2\tilde{g}$ and we approximate (19) with $\dot{\gamma}^2 \approx 6\tilde{g}^2mr^2/E = \dot{\alpha}^2$. The dissipation rate $\dot{E}$ for dry contour friction can therefore be expressed as $\dot{E} = -\frac{a}{\sqrt{E}}$ for $E > 0$ with $a = \sqrt{6}\mu_R m^{3/2}\tilde{g}^2 r^2 > 0$. For an arbitrary initial condition $E(t_0) = E_0$, this differential equation in $E$ obeys the solution

$$E(t) = \left( E_0^{\frac{3}{2}} - \frac{3}{2}a(t-t_0) \right)^{\frac{2}{3}} \quad \text{for } t_0 \le t \le t_f, \tag{20}$$

which shows (see the black line Figure 7a) a decrease to zero in a finite time $t_f - t_0 = 2E_0^{\frac{3}{2}}/(3a)$.

If we consider a viscous contour friction model $\lambda_R =$

$-c\gamma_R$, in which $c$ is the viscosity parameter, then the dissipation rate reads as $\dot{E} = -c\gamma_R^2 = -cr^2\dot{\gamma}^2$. Using the approximation $\dot{\gamma}^2 \approx \dot{\alpha}^2$, similar to the above analysis, we deduce that $\dot{E} = -\frac{a}{E}$, with $a = 6c\tilde{g}mr^3$, which obeys the solution

$$E(t) = \left(E_0^2 - 2a(t-t_0)\right)^{\frac{1}{2}} \quad \text{for } t_0 \le t \le t_f, \quad (21)$$

and shows (the grey line in Figure 7a) a decrease to zero in a finite time $t_f - t_0 = E_0^2/(2a)$.

**4.2.2 Classical rolling friction model** Classically, the resistance against rolling of two interacting bodies is modelled by a set-valued force law which relates the orthogonal projection, on the contact plane, of the relative angular velocity of the bodies $\boldsymbol{\omega}_R$, to a tangential frictional couple $\boldsymbol{M}_R$, transmitted by the contact

$$-\boldsymbol{\omega}_R \in N_{C_R}(\boldsymbol{M}_R), \quad (22)$$

with $C_R := \{\boldsymbol{v} \in \mathbb{R}^2 \mid \|\boldsymbol{v}\| \le \mu_R\lambda_N\}$. Similar to the analysis conducted with the contour friction model, we study here the total energy decrease for classical rolling friction. More generally, the set $C_R$ will be some non-circular closed convex set corresponding to an anisotropic law. The projection of angular velocity vector on the contact plane $\boldsymbol{\omega}_R$ can be decomposed along the axis $\boldsymbol{e}_x^R$ and $\boldsymbol{e}_y^R$ (Figure 6) $\boldsymbol{\omega}_R = \begin{bmatrix}\omega_x\ \omega_y\end{bmatrix}^{\mathrm{T}} = \begin{bmatrix}\dot{\beta}\ \dot{\gamma}\cos\beta\end{bmatrix}^{\mathrm{T}}$. The dissipation rate due to classical rolling friction reads as $\dot{E} = -\mu_R\lambda_N\|\boldsymbol{\omega}_R\|$. The assumptions A.1–A.4 allowed us to make the approximation $\dot{E} = -\mu_R\lambda_N|\dot{\gamma}|\cos\beta$. Substitution of (18) and $\dot{\gamma}^2 \approx \dot{\alpha}^2$ gives $\dot{E} = -a\sqrt{E}$ with $a = 2\sqrt{6}/3\mu_R\,\tilde{g}\,\sqrt{m} > 0$. For an arbitrary initial condition $E(t_0) = E_0$, this differential equation obeys the solution

$$E(t) = \left(\sqrt{E_0} - \frac{a}{2}(t-t_0)\right)^2 \text{ for } t_0 \le t \le t_f, \quad (23)$$

which shows (see the black line in Figure 7b) a decrease to zero in a finite time $t_f - t_0 = 2\sqrt{E_0}/a$.

If we consider a viscous classical rolling friction model $\boldsymbol{M}_R = -c\boldsymbol{\omega}_R$, then the dissipation rate reads as $\dot{E} = -c\|\boldsymbol{\omega}_R\|^2 = -c\dot{\gamma}^2\cos^2\beta$, in which assumption A. 2 has been used and $c$ is a viscosity parameter. Similar to the above analysis, we deduce that $\dot{E} = -aE$, with $a = \frac{8c}{3mr^2}$. For an arbitrary initial condition $E(t_0) = E_0$, this differential equation obeys the solution

$$E(t) = E_0 e^{-a(t-t_0)} \quad \text{for } t \ge t_0, \quad (24)$$

which shows (see the grey line in Figure 7b) an asymptotic behaviour of the energy and a decrease to zero is therefore not achieved in a finite time.

**4.2.3 Coulomb-Contensou friction** We assume the sliding velocity $\boldsymbol{\gamma}_T$ to be negligible. Consequently, the dissipation rate is due to the work done by the drilling torque, i.e. $\dot{E} = \lambda_\tau \cdot \gamma_\tau$, which according to (8) and the Coulomb-Contensou friction law (Section 2.3.2) leads to $\dot{E} = -\frac{3\pi}{16}\mu_F mg \cdot \epsilon|\dot{\alpha} + \dot{\gamma}\sin\beta|$, in which $\epsilon$ is the radius of the contact surface. Using (18), $\rho\sin\beta = 1$ and $\dot{\alpha} = -\rho\dot{\gamma}$ we deduce the differential equation $\dot{E} = -aE^{\frac{3}{2}}$ with $a = \frac{\pi\sqrt{2}}{4\sqrt{3}}\frac{\mu_F\epsilon}{r^2\sqrt{m}}$, which obeys the solution

$$E(t) = \left(\frac{1}{\sqrt{E_0}} + \frac{a}{2}(t-t_0)\right)^{-2} \quad \text{for } t \ge t_0, \quad (25)$$

and which shows (see the dashed line in Figure 7b) an asymptotic behaviour of the energy.

## 5 Discussion of analytical, numerical and experimental results

In this section we will discuss the analytical and numerical results (Sections 3 and 4) and compare those with experimental results which can be found in literature.

In the analytical analysis of Section 4.2, we studied the energy decrease of a rolling disk under the assumptions A.1–A.4 for various types of friction. If dry contour friction is assumed, then the analytical analysis indicates that the energy decreases in a finite time to zero, which is in accordance with the numerical simulation for Coulomb and contour friction (Leine *et al.*, 2005). Moreover, we checked that the profile of $E(t)$ during the final stage of the corresponding simulation is indeed of the form (20). If Coulomb-Contensou is assumed, then the analytical analysis indicates that the energy decreases asymptotically to zero, which is in accordance with a numerical simulation with only Coulomb-Contensou friction and the profile of $E(t)$ is indeed of the form (25). Additional simulations, not presented here, show that the numerical results for classical rolling friction are in accordance with the analytical results of Section 4.2.2. The final stage of the motion of the simulation with Coulomb-Contensou and contour friction is similar in form to the final stage of the simulation with contour friction. This can be understood from the analytical analysis of the energy decay (Section 4.2): the dissipation rate $\dot{E}$ due to contour friction increases with decreasing energy $E$, while the dissipation rate $\dot{E}$ due to Coulomb-Contensou friction decreases with decreasing energy $E$. The final stage of the motion with both Coulomb-Contensou and contour friction will therefore be dominated by the dissipation due to contour friction.

Experiments on rolling disks have been performed by (McDonald and McDonald, 2001) and (Easwar *et al.*, 2002), both presenting their results in terms of $\dot{\alpha}(t)$. McDonald and McDonald performed the experiment on a single disk using a phototransistor. Easwar et al. measured the movement of steel disks and a steel ring

on supports of various materials using a high-speed camera. The experimental data of (McDonald and McDonald, 2001) and (Easwar *et al.*, 2002) can be described for the final stage of the motion by a power law

$$\dot{\alpha}(t) \propto (t_f - t)^{-\frac{1}{n_{\exp}}}. \tag{26}$$

The experiments of (McDonald and McDonald, 2001) suggest that $n_{\exp} = 4$ and the experiments of (Easwar *et al.*, 2002) on various disk/ring–support combinations suggest that $2.7 < n_{\exp} < 3.2$.

The analytical analysis of Section 4.2 leads to the relation $6\tilde{g}^2 mr^2/E = \dot{\alpha}^2$ between $\dot{\alpha}$ and $E$

$$\dot{\alpha}(t) \propto E(t)^{-\frac{1}{2}} \propto (t_f - t)^{-\frac{1}{n_{\text{ana}}}}. \tag{27}$$

We now derive $n_{\text{ana}}$ for those friction models of Section 4.2, which lead to an energy decease to zero in a finite time. It follows from (20), that $n_{\text{ana}} = 3$ for the dry contour friction model. Similarly, it holds that $n_{\text{ana}} = 4$ for viscous contour friction. Dry classical rolling friction leads to $n_{\text{ana}} = 1$. If we now compare the experimental results with the results from the analytical model, then dry or viscous contour friction could well explain the energy decay of the experimental results. We therefore belief that contour friction is indeed the dominant mechanism of dissipation during the final stage of the motion. However, we have to keep in mind that (at least in theory) other dissipation mechanisms might exist that lead to a similar energy decay.

## 6 Conclusion

In this paper a numerical model for a rolling disk has been developed, using a parametrization with Euler parameters, which is able to take into account the unilateral contact constraints and different types of frictional models. The numerical model has proven its capability to describe the motion of objects, with a flat side of circular contour, on a plane. The numerical results seem to be reasonable for the chosen contact parameters, but a fairly small stepsize has to be taken to properly describe the motion.

An analytical analysis of the energy decay during the final stage of rolling motion has been performed in Section 4. The derived energy profiles for the different types of frictional dissipation mechanisms agree well with the corresponding numerical energy profiles. An energy decrease to zero in finite time occurs for dry contour friction and dry classical rolling friction, and, remarkably, for *viscous* contour friction. An asymptotic decrease to zero of the energy occurs for viscous classical rolling friction and (dry) Contensou friction. The analytical analysis of Section 4 gives a better understanding of the behaviour of the disk during the last stage of the numerical simulations. A comparison with available experimental results suggests that contour friction might very well be the dominant mechanism of dissipation.

The results obtained in this paper may provide a good basis for numerical treatment of more general dynamical multi-contact problems involving interaction between cylindrical and planar objects and the like.

## References


Appell, P. (1900). Sur l'intégration des équations du mouvement d'un corps pesant de révolution roulant par une arête circulaire sur un plan horizontal; cas particulier du cerceau. *Rendiconti del Circolo Matematico di Palermo* **14**, 1–6.

Borisov, A. V., I. S. Mamaev and A. A. Kilin (2003). Dynamics of rolling disk. *Regular and Chaotic Dynamics* **8**(2), 201–212.

Easwar, K., F. Rouyer and N. Menon (2002). Speeding to a stop: The finite-time singularity of a spinning disk. *Physical Review E*.

Glocker, Ch. (2001). *Set-Valued Force Laws, Dynamics of Non-Smooth Systems*. Vol. 1 of *Lecture Notes in Applied Mechanics*. Springer-Verlag. Berlin.

Jean, M. (1999). The non smooth contact dynamics method. *Computer Methods in Applied Mechanics and Engineering* **177**, 235–257.

Kessler, P. and O. M. O'Reilly (2002). The ringing of Euler's disk. *Regular and Chaotic Dynamics* **7**(1), 49–60.

Leine, R. I. and Ch. Glocker (2003). A set-valued force law for spatial Coulomb–Contensou friction. *European Journal of Mechanics – A/Solids* **22**, 193–216.

Leine, R. I. and H. Nijmeijer (2004). *Dynamics and Bifurcations of Non-Smooth Mechanical Systems*. Vol. 18 of *Lecture Notes in Applied and Computational Mechanics*. Springer-Verlag. Berlin-Heidelberg-New York.

Leine, R. I., C. Le Saux and Ch. Glocker (2005). Dynamics of a rolling disk in the presence of dry friction. *Journal of Nonlinear Science*. in press.

McDonald, A. J. and K. T. McDonald (2001). The rolling motion of a disk on a horizontal plane. *Preprint, Princeton High School, New Jersey*.

Moffatt, H. K. (2000). Euler's disk and its finite-time singularity. *Nature* **404**, 833–834.

Moreau, J. J. (1988). Unilateral contact and dry friction in finite freedom dynamics. In: *Non-Smooth Mechanics and Applications* (J. J. Moreau and P. D. Panagiotopoulos, Eds.). Vol. 302 of *CISM Courses and Lectures*. pp. 1–82. Springer. Wien.

O'Reilly, O. M. (1996). The dynamics of rolling disks and sliding disks. *Nonlinear Dynamics* **10**(3), 287–305.

Stanislavsky, A. A. and K. Weron (2001). Nonlinear oscillations in the rolling motion of Euler's disk. *Physica D* **156**, 247–259.